1991

# Onset of convection for autocatalytic reaction fronts: Laterally unbounded system

Boyd F. Edwards

Joseph W. Wilder

Kenneth Showalter

1-1991

# Onset of Convection for Autocatalytic Reaction Fronts: Laterally Unbounded System

Boyd F. Edwards
*Utah State University*

J. W. Wilder

K. Showalter



Recommended Citation
"Onset of Convection for Autocatalytic Reaction Fronts: Laterally Unbounded System," B. F. Edwards, J. W. Wilder, and K. Showalter, Phys. Rev. A 43, 749 (1991) [60].

# Onset of convection for autocatalytic reaction fronts: Laterally unbounded system

Boyd F. Edwards, Joseph W. Wilder, and Kenneth Showalter
*Department of Physics, Department of Mathematics, and Department of Chemistry, West Virginia University, Morgantown, West Virginia 26506*

(Received 29 May 1990; revised manuscript received 19 September 1990)

The linear stability of exothermic autocatalytic reaction fronts that convert unreacted fluid into a lighter reacted fluid is considered using the viscous thermodynamic equations. For upward front propagation and a thin front, the discontinuous jump in density at the front is reminiscent of the Rayleigh-Taylor problem of an interface between two immiscible fluids, whereas the vertical thermal gradient near the front is reminiscent of the Rayleigh-Bénard problem of a fluid layer heated from below. The problem is also similar to flame propagation, except that here the front propagation speed is limited by catalyst diffusion rather than by activation kinetics. For a thin ascending front and small density changes in a laterally unbounded system, the curvature dependence of the front speed stabilizes perturbations with short wavelengths $\lambda < \lambda_c$, whereas long wavelengths are unstable to convection, indicating that the density discontinuity dominates over thermal gradients. Simple analytical results for the critical wavelength $\lambda_c$ for onset of convection, the growth rate near onset of convection, and the maximum growth rate are found. Agreement with experiments on iodate–arsenous acid solutions in vertical tubes motivates linear and nonlinear calculations in cylindrical geometries.

## I. INTRODUCTION

Recent experiments observe steady axisymmetric convection[1–3] near iodate–arsenous acid reaction fronts in long vertical tubes. In these experiments, a thin autocatalytic reaction front converts the unreacted aqueous solution into a reacted solution of lower density, so that upward propagation of a horizontal front is potentially unstable under the action of gravity. Indeed, data for upward propagation in long vertical tubes indicate that convection becomes increasingly important as the tube diameter increases. For diameters less than a critical diameter $d_c$ of about 1 mm, the upward propagation speed is the same as the downward propagation speed and the front is flat, indicating the absence of convection. Whereas the downward propagation speed is independent of tube diameter, the upward propagation speed and the corresponding curvature of the front (Fig. 1) increase with the tube diameter as the diameter is raised above the critical diameter, indicating increasing amounts of steady convection. This steady convection can become unstable at diameters larger than about 5 mm. Existing reaction-diffusion theory for such systems[4] omits convection.

The goal of this paper is to develop a theory of convection for autocatalytic fronts. Of particular interest is to investigate how this problem fits into the class of fluid problems exhibiting transitions to chaos. Since the reacted and unreacted fluids have different densities in general, the problem is similar to the classical Rayleigh-Taylor problem[5] of the stability of a horizontal impermeable interface between two immiscible fluids of different densities. The difference is that the front interface for autocatalytic fronts is permeable; the conversion of unreacted to reacted fluid at the front requires that fluid pass through the front. Since the chemical reaction is typically exothermic, upward propagation also produces a vertical thermal gradient in the vicinity of the front, leading to a potentially unstable density gradient [Fig. 1(a)]. This gradient might drive thermal convection reminiscent of Rayleigh-Bénard convection of a fluid layer heated from

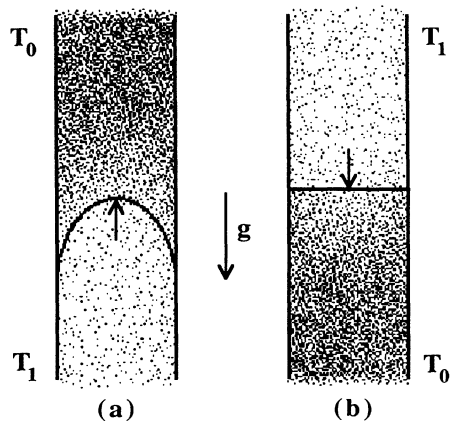


FIG. 1. Schematic representation of the front shape for (a) ascending and (b) descending autocatalytic reaction fronts in a vertical tube of diameter greater than the critical diameter for the onset of convection. For exothermic reactions, the final temperature $T_1$ of the reacted fluid exceeds the initial temperature $T_0$ of the unreacted fluid, leading to potentially unstable density gradients for upward propagation. Density gradients due to both thermal expansion in the unreacted fluid and to differences in composition of the reacted and unreacted fluids are represented schematically by the density of dots.

 

below.[6-10] The problem is also similar to flame propagation,[11-15] the principal difference being in the mechanism for propagation of the front. Flame propagation occurs only when the temperature of the gas near the flame is sufficiently high, so that nonlinear activation kinetics and thermal diffusion typically determine the flame speed. In the present problem, the slow diffusion of the catalyst species limits the front speed,[4,16] implying a chemically thin reaction front and significant thermal diffusion into the unreacted fluid. Free convection produced by a dense solution diffusing downward into a less dense solution in a vertical tube[2,3,17,18] (such as for a salinity gradient) involves a uniform density gradient which is absent in autocatalytic systems.

In this paper, we introduce and justify a thin reaction front approximation similar to approximations used in flame propagation[11-15] and a uniform-density approximation analogous to the Oberbeck-Boussinesq approximation[19] for Rayleigh-Bénard convection. These include a temperature gradient jump (boundary) condition at the front similar to a condition used in solidification theory.[20] In the thin-front approximation, we find that all chemical kinetics can be subsumed into a temperature difference and a planar front speed available from experiments, so that an equation for molecular diffusion is unnecessary. Using the resulting theory, we study the linear stability of an ascending flat front in a laterally unbounded geometry. Finally, we compare the results with experiments on iodate–arsenous acid systems and motivate the extension of the theory to cylindrical geometries. The theory presented here may also be relevant to convection in iron(II)–nitric acid reaction fronts,[21,22] liquid-liquid phase transitions, and convection during solidification.

## II. FLUID DENSITY AND FRONT STRUCTURE

Small density changes in the fluid arise from thermal expansion and from differences in chemical composition between the reacted and unreacted fluids. Since these changes are small, we can write first-order Taylor expansions in the unreacted fluid,

$$\rho(T)=\rho_1+\left[\frac{\partial\rho}{\partial T}\right]_{T_1}(T-T_1)+\cdots$$
$$=\rho_1[1-\alpha(T-T_1)]\ , \qquad (1)$$

and in the reacted fluid,

$$\rho(T)=\tilde{\rho}_1[1-\alpha(T-T_1)]\ . \qquad (2)$$

Here $\rho_1$ and $\tilde{\rho}_1$ are the densities of the unreacted and reacted fluids at a reference temperature $T_1$, taken to be the final temperature of the reacted fluid (Fig. 1), and $\alpha=-\rho_1^{-1}(\partial\rho/\partial T)_{T_1}$ is the classical thermal expansion coefficient at constant pressure, taken to be the same in the reacted fluid as in the unreacted fluid. An isothermal fractional difference between these densities

$$\delta_1=\rho_1/\tilde{\rho}_1-1 \qquad (3)$$

is defined so that $\delta_1>0$ if the unreacted fluid has the higher density. We also define an overall fractional density difference involving the unreacted fluid density $\rho_0$ far ahead of the front at initial temperature $T_0$ (Fig. 1);

$$\delta_0=\rho_0/\tilde{\rho}_1-1$$
$$=\delta_1+(1+\delta_1)\alpha\Delta T$$
$$=\delta_1+\alpha\Delta T\ . \qquad (4)$$

The second equality follows by substituting Eq. (1) for $\rho_0=\rho(T_0)$ and by defining an overall adiabatic temperature difference $\Delta T=T_1-T_0$.

The equations of state [Eqs. (1) and (2)], the assumption that $\alpha$ is the same in the reacted and unreacted fluids, and the third equality in Eq. (4) are all valid to first order in the thermal and compositional density corrections $\alpha\Delta T$ and $\delta_1$. These are well justified for iodate–arsenous acid systems where $\delta_1\approx\alpha\Delta T\approx 1\times10^{-4}$ (Table I). We note that in such systems, both the correction $\delta_1$ due to density differences between the reacted and unreacted fluids and the correction $\alpha\Delta T$ due to thermal expansion are positive. Positive $\delta_0=\delta_1+\alpha\Delta T$ therefore places the lighter reacted fluid below the heavier fluid for upward propagation in these systems, leading to potential instability and convection under the action of gravity, whereas downward propagation leads to no instability. Below, these small density corrections are neglected consistently except where they modify gravity, that is, except where they provide the essential gravitational instability leading to convection. A separate calculation,[23] which includes all of the composition-induced density corrections, yields results that differ by less than 0.1% from the results obtained below. The general theory developed in this paper also applies to other systems where $\delta_1$ and $\alpha\Delta T$ can have either sign.[22,24]

It is helpful to consider the thickness of the reaction front separating the reacted fluid from the unreacted fluid in autocatalytic systems such as the iodate–arsenous acid system. In contrast with flame propagation[11-15] where the unreacted fluid must be heated before reaction can occur, the front propagation speed in autocatalytic systems is limited by the slow diffusion of a catalyst species into the unreacted fluid. Since the thermal diffusivity $D_T$ is typically much larger than the catalyst molecular diffusivity $D_C$ in these systems, the heat produced in the chemical reaction front diffuses well ahead of the reaction front into the unreacted fluid, thereby producing thermal gradients in a layer of thickness[4,16] $d_T=D_T/c_0$, where the planar front speed $c_0$ is limited by catalyst diffusion.[4,16] For iodate–arsenous acid systems (Table I), the reaction front thickness $d_r=D_C/c_0\approx7\times10^{-3}$ cm is small compared to the thermal front thickness $d_T\approx0.5$ cm. Furthermore, the reaction front is also thin compared to typical experimental tube diameters $d\approx0.1$ cm. In contrast with Rayleigh-Bénard convection[6-10] and Taylor-vortex flow,[7,25] the thermal length scale $d_T$ is independent of any externally imposed boundaries.

A thin-front approximation that treats the reaction front as a surface separating the reacted and unreacted fluids is useful when the reaction front thickness is small compared to other length scales in the problem. In this approximation, we can define a time-dependent height

$z=H(x,y,t)$ of the front and a unit vector $\hat{\mathbf{n}}$ pointing normal to the front into the unreacted fluid (Fig. 2). In the uniform-density approximation, the fluid velocity $\mathbf{V}$ is continuous at the front. Consequently, the normal front velocity relative to the moving fluid,

$$c=\hat{\mathbf{n}}\cdot\hat{\mathbf{z}}\frac{\partial H}{\partial t}-\hat{\mathbf{n}}\cdot\mathbf{V}|_{z=H}\ , \tag{5}$$

involves the normal fluid velocity at the front $\hat{\mathbf{n}}\cdot\mathbf{V}_{z=H}$ and the normal front velocity $\hat{\mathbf{n}}\cdot\hat{\mathbf{z}}\partial H/\partial t$ in the laboratory frame.

The relative normal velocity $c$ gives the volume of unreacted fluid consumed per unit front surface area per unit time, which depends on the curvature $K$ according to[26]

$$c=c_0+D_C K\ , \tag{6}$$

called the eikonal velocity. Here $K$ is measured as positive where the center of curvature is in the unreacted fluid. Thus, for ascending fronts with the unreacted fluid above the reacted fluid, positive curvature increases the front speed $c$ where the front is concave upward (in valleys) and negative curvature decreases the front speed where the front is concave downward (at peaks). This curvature dependence of the front speed therefore tends to flatten nonplanar reaction fronts with time. As will be seen, this effect stabilizes short-wavelength perturbations about flat fronts, and is therefore crucial to the understanding of onset of convection in autocatalytic systems.

A useful relation between the unit front normal vector $\hat{\mathbf{n}}$ and the (horizontal) front gradient $\nabla H(x,y,t)$,

$$\hat{\mathbf{n}}=\pm\frac{(\hat{\mathbf{z}}-\nabla H)}{|\hat{\mathbf{z}}-\nabla H|}=\pm\frac{(\hat{\mathbf{z}}-\nabla H)}{(1+|\nabla H|^2)^{1/2}}\ , \tag{7}$$

follows from the observation that $\hat{\mathbf{n}}$ has a slope of magnitude $|\nabla H|^{-1}$ in the vertical plane containing both $\hat{\mathbf{n}}$ and

TABLE I. Parameter values relevant to convection in iodate–arsenous acid systems.

| Parameter | Description | Value |
|---|---|---|
| $T_0$ | initial temperature of unreacted fluid | 25 °C |
| $T_1$ | final temperature of reacted fluid | |
| $\Delta T=T_1-T_0$ | overall temperature difference | 0.40 °C [a] |
| $\alpha$ | thermal expansion coefficient | $2.57\times10^{-4}$/°C [b] |
| $\Delta\theta=\alpha\Delta T$ | dimensionless temperature difference | $1.03\times10^{-4}$ |
| $\tilde{\rho}_1$ | density of reacted fluid at $T_1$ | 1.00 g/cm$^3$ |
| $\rho_1$ | density of unreacted fluid at $T_1$ | |
| $\rho_0$ | density of unreacted fluid at $T_0$ | |
| $\delta_1=\rho_1/\tilde{\rho}_1-1$ | density difference at $T_1$ | $0.87\times10^{-4}$ [c] |
| $\delta_0=\rho_0/\tilde{\rho}_1-1$ $=\delta_1+\Delta\theta$ | overall density difference | $1.9\times10^{-4}$ |
| $c_p$ | isobaric specific heat | 1 cal/°C g |
| $c_0$ | flat-front propagation speed | $2.95\times10^{-3}$ cm/s [d] |
| $D_T$ | thermal diffusivity | $1.45\times10^{-3}$ cm$^2$ s$^{-1}$ [e] |
| $D_C$ | catalyst diffusivity | $2.0\times10^{-5}$ cm$^2$ s$^{-1}$ [f] |
| $d_T=D_T/c_0$ | thermal front thickness | 0.49 cm |
| $d_r=D_C/c_0$ | chemical reaction front thickness | $6.8\times10^{-3}$ cm |
| $\nu$ | kinematic viscosity | $9.2\times10^{-3}$ cm$^2$ s$^{-1}$ [g] |
| $g$ | acceleration of gravity | 980 cm/s$^2$ |
| $\mathcal{G}=g\nu c_0^{-3}$ | dimensionless acceleration of gravity | $3.51\times10^8$ |
| $\mathcal{D}_T=D_T/\nu$ | dimensionless thermal diffusivity | 0.158 |
| $\mathcal{D}_C=D_C/\nu$ | dimensionless catalyst diffusivity | $2.17\times10^{-3}$ |
| $\mathcal{P}=\mathcal{D}_T^{-1}$ | Prandtl number | 6.34 |
| $\mathcal{L}=\mathcal{D}_T/\mathcal{D}_C$ | Lewis number | 72.5 |
| $\mathcal{R}=\Delta\theta\mathcal{G}\mathcal{D}_T^2$ $=g\alpha\Delta T d_T^3/D_T\nu$ | Rayleigh number | 898 |

[a]Follows from Eq. (11) with latent heat $L=-\Delta H[IO_3^-]$, enthalpy $\Delta H=-80$ kcal/mol (Ref. 1, Sec. 3.4.2), iodate molar concentration $[IO_3^-]=5.0\times10^{-3}M$ [Table 3 of Ref. 3 (corresponding to Table 3.1 of Ref. 1), reaction mixture $A$, where $M$ signifies moles per liter of solution], and values of $\rho_1\approx\tilde{\rho}_1$ and $c_p$ from this table. The corresponding chemical concentrations are $[H_3AsO_3]=29.8\times10^{-3}M$, $[KIO_3]=5.0\times10^{-3}M$, $[H^+]=10.0\times10^{-3}M$, and $[I^-]<0.0001\times10^{-3}M$ (Table 3 of Ref. 3).

[b]Reference 28.

[c]This value for reaction mixture $A$ follows from Table 3 in Ref. 3, based on the value $\delta_1=1.3\times10^{-4}$ for reaction mixture $D$ deduced from Fig. 4c of Ref. 3 (corresponding to reaction mixture $F$ and Fig. 3.6 of Ref. 1) and the assumption that $\delta_1$ is proportional to the iodate concentration.

[d]From Table 4 of Ref. 3 (corresponding to Table 3.4 of Ref. 1).

[e]Reference 1, Sec. 3.4.3 (or Ref. 3).

[f]Reference 1, Sec. 3.4.3 (or Ref. 3), for iodate catalyst.

[g]Interpolated from Table VI, Ref. 9.

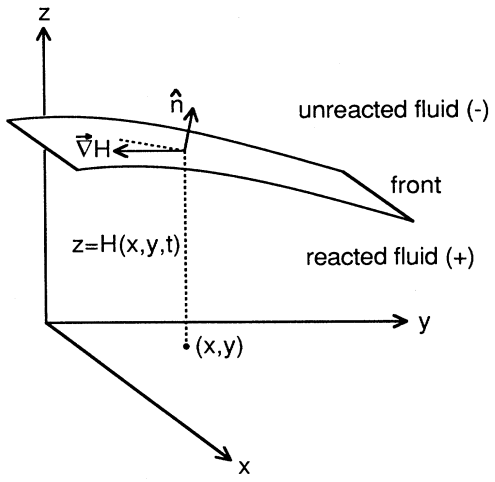


FIG. 2. Coordinate system used in the calculations with a front surface $z=H(x,y,t)$, a front normal vector $\hat{\mathbf{n}}$ pointing into the unreacted fluid, and a $z$ axis pointing up.

$\nabla H$ (Fig. 2). Here the + sign accounts for upward propagation (with the unreacted fluid above the front) and the − sign accounts for downward propagation.

The wave nature of the reaction front implies a slope dependence of the vertical front velocity. In the absence of any fluid motion or curvature corrections, the normal front velocity $\hat{\mathbf{n}}\cdot\hat{\mathbf{z}}\partial H/\partial t=c_0$ is constant and the radius of curvature of a peak in an ascending front increases with time as the front propagates farther from the center of curvature of the peak, in such a way that spherical waves remain spherical with time in accordance with Huygen's principle for wave propagation. Accordingly, the vertical front velocity $\partial H/\partial t=c_0(1+|\nabla H|^2)^{1/2}$ at fixed horizontal position increases with increasing slope $|\nabla H|$ and takes its smallest value where $|\nabla H|=0$. This slope dependence of the vertical front velocity is distinct from the curvature dependence of the normal front velocity discussed above, and is expected to be important in finite-amplitude convection.

Steady propagation of a nonplanar front means that $\partial H/\partial t$ is independent of horizontal position while $H$, $K$, and $\nabla K$ depend on horizontal position. For this situation, Eq. (5) demands a nonuniform fluid velocity $\mathbf{V}|_{z=H}$ to balance slope and curvature effects. Thus steady propagation of a curved front cannot be maintained without fluid convection. As a result, an expansion in the amplitude of the deviations from a planar front is expected to be equivalent to a convective amplitude expansion familiar in fluid dynamics.[8] We intend to perform such an amplitude expansion in subsequent work.

## III. EQUATIONS OF MOTION

The thermohydrodynamic equations of motion expressing conservation of momentum, energy, and mass[9,27] are invariant under transformations to coordinate frames moving with constant speed with respect to the laboratory frame. It is convenient to evaluate these equations in a frame moving with the front:

$$\frac{\partial \mathbf{V}}{\partial t}+(\mathbf{V}\cdot\nabla)\mathbf{V}=-\frac{\rho}{\rho_1}g\hat{\mathbf{z}}-\frac{1}{\rho_1}\nabla P+\nu\nabla^2\mathbf{V}\ , \tag{8a}$$

$$\frac{\partial T}{\partial t}+\mathbf{V}\cdot\nabla T=D_T\nabla^2 T+\Phi\ , \tag{8b}$$

$$\nabla\cdot\mathbf{V}=0\ . \tag{8c}$$

Length, time, temperature, and pressure scales $d\approx 1$ mm (the tube diameter), $d/c_0$, $\Delta T$, and $\rho g d$ along with values from Table I imply that the gravity and pressure terms in Eq. (8a) are of order $10^5$–$10^7$ relative to the remaining terms in the equation. Accordingly, we have set $\rho=\rho_1$ everywhere except in the gravity term consistent with the uniform-density approximation. We can neglect heat generation due to viscous dissipation because the corresponding term

$$\Phi=-(2\rho c_p)^{-1}\sum_{i,j=1}^{3}T_{ij}^V$$

in Eq. (8b) is of relative order $10^{-12}$. Here

$$T_{ij}^V=-\nu\rho_1\left[\frac{\partial V_i}{\partial x_j}+\frac{\partial V_j}{\partial x_i}\right] \tag{9}$$

is the viscous stress tensor and $c_p$ is the isobaric specific heat of the fluid. The kinematic viscosity $\nu$ is taken to be the same in the unreacted and reacted fluids, consistent with the very small chemical concentrations in the aqueous solutions in the experiments (of order $5\times10^{-3}$ moles per liter of solution; see note a of Table I). Furthermore, experimental data[9] imply negligible temperature corrections to $\nu$ and $D_T$ smaller than 1% for typical room-temperature experiments with temperature differences $\Delta T\approx 0.4$ K (Table I).

The uniform-density approximation demands continuous fluid velocity $\mathbf{V}$ and continuous stress $n_j T_{ij}$ at the interface between the reacted and unreacted fluids, where the $n_j$ are Cartesian components of the unit vector, repeated indices are summed, and the stress tensor $T_{ij}=P\delta_{ij}+T_{ij}^V$ involves the Kronecker delta function $\delta_{ij}$. Continuous stress at the interface implies a balance between the forces of the reacted and unreacted fluids on an interface area element $dA$. Conservation of energy at the interface requires a discontinuity in the normal derivative of the temperature,

$$Lc=k_T[\hat{\mathbf{n}}\cdot\nabla T]_-^+\ , \tag{10}$$

where $[q]_-^+=q_+-q_-$ denotes the difference between the values of a quantity $q$ on the reacted (+) and unreacted (−) sides of the front. Here

$$L=\rho_1 c_p\Delta T \tag{11}$$

is the latent heat liberated by the reaction per unit volume of unreacted solution in the uniform-density approximation, so that $Lc$ is the energy per unit area per unit time produced by the moving reaction front. The quantity $k_T[\hat{\mathbf{n}}\cdot\nabla T]_-^+$ gives the corresponding net heat current density leaving the front by thermal diffusion and involves the thermal conductivity $k_T=D_T\rho_1 c_p$. Since

bulk fluid motion does not affect the rate of conversion of reactants to products, the left side of Eq. (10) requires the eikonal velocity $c=c_0+D_C K$ rather than the total normal velocity $\hat{\mathbf{n}}\cdot\hat{\mathbf{z}}\partial H/\partial t$, which includes fluid motion. Here we have neglected any differences in $c_p$ and $D_T$ between the reacted and unreacted fluids, consistent with the small chemical concentrations in the experiments. Equation (10) is analogous to the temperature gradient discontinuity condition required at moving solidification fronts,[20] except that here the normal front velocity, instead of the temperature, is a known function of the front curvature. Local thermal equilibrium requires that the temperature be continuous at the interface, thus completing the necessary interface conditions. A careful analysis of these interface conditions[23] shows that they are valid for steady flows in the frame of the moving front, consistent with steady flows in the moving frame and with mildly nonsteady flows near criticality as long as $c_0^{-1}\partial H/\partial t \ll 1$.

To account for the composition-induced discontinuity in the density, it is convenient to define a reduced pressure (see Ref. 12, for example)

$$P_r=P+\gamma\rho_1 gz \ , \tag{12}$$

where $\gamma=1$ in the unreacted fluid and $\gamma=\tilde{\rho}_1/\rho_1=1-\delta_1$ in the reacted fluid to first order in $\delta_1$. Accordingly, a complete set of equations governing convection in autocatalytic systems in the thin-front and uniform-density approximations includes the dynamic equations

$$\frac{\partial\mathbf{V}}{\partial t}+(\mathbf{V}\cdot\nabla)\mathbf{V}=-\gamma g\alpha(T_1-T)\hat{\mathbf{z}}-\frac{1}{\rho_1}\nabla P_r+\nu\nabla^2\mathbf{V} \ , \tag{13a}$$

$$\frac{\partial T}{\partial t}+\mathbf{V}\cdot\nabla T=D_T\nabla^2 T \ , \tag{13b}$$

$$\nabla\cdot\mathbf{V}=0 \ , \tag{13c}$$

$$\hat{\mathbf{n}}\cdot\hat{\mathbf{z}}\frac{\partial H}{\partial t}=c_0+D_C K+\hat{\mathbf{n}}\cdot\mathbf{V}|_{z=H} \ , \tag{13d}$$

and the jump conditions

$$[\hat{\mathbf{n}}\cdot\mathbf{V}]_-^+=0 \ , \tag{13e}$$

$$[\hat{\mathbf{n}}\times\mathbf{V}]_-^+=0 \ , \tag{13f}$$

$$[P_r]_-^+=-\delta_1\rho_1 gH-[n_i n_j T_{ij}^V]_-^+ \ , \tag{13g}$$

$$[\epsilon_{ijk}n_j n_l T_{kl}^V]_-^+=0 \ , \tag{13h}$$

$$[\hat{\mathbf{n}}\cdot\nabla T]_-^+=D_T^{-1}\Delta T(c_0+D_C K) \ , \tag{13i}$$

$$[T]_-^+=0 \ , \tag{13j}$$

where the jump in reduced pressure depends on the acceleration of gravity and the totally antisymmetric tensor $\epsilon_{ijk}$ appears in the tangential stress condition, Eq. (13h). An eikonal velocity (instead of activation kinetics) and nonzero viscosity distinguish Eqs. (13) from the equations typically used for flame propagation.[11–14] Equations (13) also differ substantially from a set of equations for viscous flame propagation in a boundary-layer approximation.[15] A stabilizing curvature term in Eq. (13d) renders the convectionless front velocity nonuniform, whereas a stabilizing surface tension term renders the stress discontinuous in the viscous Rayleigh-Taylor problem.[5] In contrast to (convectionless) reaction-diffusion theory,[4] which requires a chemical diffusion equation to resolve the reaction front, our thin-front treatment relegates the reaction kinetics to the experimental parameters $c_0$ and $\Delta T$, thus simplifying the analysis. In the thin-front approximation, knowledge of the chemical compositions of the fluids is therefore unnecessary.

It is convenient to use length and time scales $\nu c_0^{-1}$ and $\nu c_0^{-2}$ to define dimensionless coordinates $\mathbf{x}^*$ and $t^*$ by the relations $\mathbf{x}=\nu c_0^{-1}\mathbf{x}^*$ and $t=\nu c_0^{-2}t^*$. We also define dimensionless functions by

$$T(\mathbf{x},t)=T(\nu c_0^{-1}\mathbf{x}^*,\nu c_0^{-2}t^*)=\alpha^{-1}\theta(\mathbf{x}^*,t^*) \ ,$$

$$P_r(\mathbf{x},t)=\rho_1 c_0^2 p(\mathbf{x}^*,t^*) \ ,$$

$$K(\mathbf{x},t)=c_0\nu^{-1}\kappa(\mathbf{x}^*,t^*) \ ,$$

$$\mathbf{V}(\mathbf{x},t)=c_0\mathbf{v}(\mathbf{x}^*,t^*) \ ,$$

$$H(\mathbf{x},t)=\nu c_0^{-1}h(\mathbf{x}^*,t^*) \ .$$

Convenient dimensionless parameters include a dimensionless acceleration of gravity $\mathcal{G}=g\nu c_0^{-3}$, thermal diffusivity $\mathcal{D}_T=D_T/\nu$, and catalyst diffusivity $\mathcal{D}_C=D_C/\nu$. With $\Delta\theta=\alpha\Delta T=\delta_0-\delta_1$ from Eq. (4), these parameters can be related to the well-known Prandtl number $\mathcal{P}=\mathcal{D}_T^{-1}$, Lewis number $\mathcal{L}=\mathcal{D}_T/\mathcal{D}_C$, and Rayleigh number $\mathcal{R}=\Delta\theta\mathcal{G}\mathcal{D}_T^2=g\alpha\Delta T d_T^3/D_T\nu$ for convection driven by thermal gradients near the front. Table I summarizes these parameter definitions and gives typical values for iodate–arsenous acid systems.

We can now write Eqs. (13) in dimensionless form, with equations of motion

$$\frac{\partial\mathbf{v}}{\partial t}+(\mathbf{v}\cdot\nabla)\mathbf{v}=-\gamma(\theta_1-\theta)\mathcal{G}\hat{\mathbf{z}}-\nabla p+\nabla^2\mathbf{v} \ , \tag{14a}$$

$$\frac{\partial\theta}{\partial t}+\mathbf{v}\cdot\nabla\theta=\mathcal{D}_T\nabla^2\theta \ , \tag{14b}$$

$$\nabla\cdot\mathbf{v}=0 \ , \tag{14c}$$

$$\hat{\mathbf{n}}\cdot\hat{\mathbf{z}}\frac{\partial h}{\partial t}=1+\mathcal{D}_C\kappa+\hat{\mathbf{n}}\cdot\mathbf{v}|_{z=h} \ ; \tag{14d}$$

jump conditions

$$[\hat{\mathbf{n}}\cdot\mathbf{v}]_-^+=0 \ , \tag{14e}$$

$$[\hat{\mathbf{n}}\times\mathbf{v}]_-^+=0 \ , \tag{14f}$$

$$[p]_-^+=-\delta_1\mathcal{G}h-[n_i n_j T_{ij}^v]_-^+ \ , \tag{14g}$$

$$[\epsilon_{ijk}n_j n_l T_{kl}^v]_-^+=0 \ , \tag{14h}$$

$$[\hat{\mathbf{n}}\cdot\nabla\theta]_-^+=\Delta\theta\mathcal{D}_T^{-1}(1+\mathcal{D}_C\kappa) \ , \tag{14i}$$

$$[\theta]_-^+=0; \tag{14j}$$

and corresponding dimensionless forms of the viscous stress tensor

$$T_{ij}^v=-\frac{\partial v_i}{\partial x_j}-\frac{\partial v_j}{\partial x_i} \tag{14k}$$

and unit normal vector [from Eq. (7)]

$$\hat{n}=\pm\frac{(\hat{\mathbf{z}}-\nabla h)}{(1+|\nabla h|^2)^{1/2}}\ , \tag{14l}$$

where we have dropped the asterisks from the dimensionless independent variables.

## IV. LINEAR STABILITY OF FLAT HORIZONTAL FRONTS

As is true for the Rayleigh-Bénard problem,[8,9] a laterally unbounded system constitutes the simplest nontrivial geometry in which to study convection for autocatalytic systems. The calculation presented below of the growth rates of small perturbations about an ascending flat front predicts a critical wavelength for the onset of convection below which curvature stabilizes the front. This critical wavelength should agree roughly with the experimental critical diameter for onset of convection in vertical tubes (near 1 mm for iodate–arsenous acid systems). Thus, this calculation provides an important first test of the theory.

In a coordinate frame fixed to an ascending horizontal front, we choose $z=h=0$ as the location of the undisturbed front, so that $z>0$ locates the unreacted fluid. In this frame, Eqs. (14) yield a steady dimensionless fluid velocity and temperature profile for the undisturbed flat front (with $\kappa=0$)

$$\mathbf{v}^{(0)}=-\hat{\mathbf{z}}\ , \tag{15a}$$

$$\theta^{(0)}=\begin{cases}\theta_0+\Delta\theta e^{-z/\mathcal{D}_T}, & z>0\\ \theta_1, & z<0\ .\end{cases} \tag{15b}$$

As before, the dimensionless temperature difference $\Delta\theta=\theta_1-\theta_0$ involves the dimensionless final and initial temperatures $\theta_1=\alpha T_1$ and $\theta_0=\alpha T_0$. Thus, since all heat is released at the reaction front at $z=0$, the temperature $\theta_1$ of the reacted fluid is uniform, and thermal diffusion yields an exponential temperature profile in the unreacted fluid with a length scale given by the dimensionless thermal diffusivity $\mathcal{D}_T$. Thus $\theta_1$ is the temperature at the undisturbed front. Since the dimensionless velocity $\mathbf{v}^{(0)}=-\hat{\mathbf{z}}$ is measured in the moving frame in units of the flat-front propagation speed $c_0$, its value corresponds to zero fluid motion in the laboratory frame.

We can now study the linear stability of the ascending flat front by introducing small time-dependent perturbations according to

$$\begin{aligned}h&=h^{(1)}\ ,\\ \mathbf{v}&=\mathbf{v}^{(0)}+\mathbf{v}^{(1)}\ ,\\ \theta&=\theta^{(0)}+\theta^{(1)}\ ,\\ p&=p^{(0)}+p^{(1)}\ .\end{aligned} \tag{16}$$

Substituting these relations into Eqs. (14) and retaining terms linear in the perturbations yields a linear homogeneous system, implying that we can introduce a perturbation wave number $q$ and growth rate $\sigma$ and endow the perturbations with exponential dependences $e^{iqx+\sigma t}$. For two-dimensional $y$-independent velocity perturbations $\mathbf{v}^{(1)}=u^{(1)}\hat{\mathbf{x}}+w^{(1)}\hat{\mathbf{z}}$ and the corresponding curvature

$$\kappa=\frac{1}{(1+|\nabla h|^2)^{1/2}}\frac{d^2h}{dx^2}\ , \tag{17}$$

Eqs. (14) yield

$$u^{(1)}=iq^{-1}\partial w^{(1)}\ , \tag{18a}$$

$$p^{(1)}=q^{-2}(\partial^2+\partial-q^2-\sigma)\partial w^{(1)}\ , \tag{18b}$$

$$(\partial^2-q^2)(\partial^2+\partial-q^2-\sigma)w^{(1)}-q^2\gamma\mathcal{G}\theta^{(1)}=0\ , \tag{18c}$$

$$(\mathcal{D}_T\partial^2+\partial-\mathcal{D}_Tq^2-\sigma)\theta^{(1)}-[\partial\theta^{(0)}]w^{(1)}=0\ , \tag{18d}$$

$$w^{(1)}|_{z=h}=(\sigma+\mathcal{D}_Cq^2)h^{(1)}\ , \tag{18e}$$

$$[w^{(1)}]^+_-=0\ , \tag{18f}$$

$$[\partial w^{(1)}]^+_-=0\ , \tag{18g}$$

$$[\partial^2w^{(1)}]^+_-=0\ , \tag{18h}$$

$$[\partial^3w^{(1)}]^+_-=-\delta_1q^2\mathcal{G}h^{(1)}\ , \tag{18i}$$

$$[\partial\theta^{(1)}]^+_-=-q^2\Delta\theta\mathcal{D}_T^{-1}\mathcal{D}_Ch^{(1)}\ , \tag{18j}$$

$$[\theta^{(1)}]^+_-=0\ . \tag{18k}$$

These equations govern the time evolution of the dimensionless perturbations about a flat front. Evidently, the vertical velocity $w^{(1)}$ and its first and second normal derivatives are continuous at the front.

### A. Infinite thermal diffusivity

Instructive analytical results can be obtained for $\mathcal{D}_T\to\infty$, where heat currents respond instantaneously to any thermal gradients, yielding a uniform undisturbed temperature profile $\theta^{(0)}=\theta_1$ from Eq. (15). Accordingly, the fluid density is piecewise uniform, with values $\rho_1$ and $\tilde{\rho}_1$ in the unreacted and reacted fluids, respectively. Hence, for infinite thermal diffusivity, the convective instability is governed solely by a discontinuous jump in density at the front characterized by the fractional density difference $\delta_1=\rho_1/\tilde{\rho}_1-1$, and involves no thermal gradients near the front.

Requiring $\theta^{(1)}|_{z=\pm\infty}=0$ (since $\theta^{(0)}$ satisfies the temperature boundary conditions at $z=\pm\infty$), setting $\mathcal{D}_T\to\infty$, and using Eqs. (18d), (18j), and (18k) yields $\theta^{(1)}=0$ and a simpler form for Eq. (18c),

$$(\partial^2-q^2)(\partial^2+\partial-q^2-\sigma)w^{(1)}=0\ . \tag{19}$$

Consequently, requiring $w^{(1)}|_{z=\pm\infty}$ to be bounded dictates the general form of the solution for the vertical velocity,

$$w^{(1)}=e^{iqx+\sigma t}\times\begin{cases}Ae^{-qz}+Be^{k_-z}, & z>0\\ Ce^{qz}+De^{k_+z}, & z<0\ ,\end{cases} \tag{20}$$

with wave numbers

$$k_\pm=-\tfrac{1}{2}\pm(\tfrac{1}{4}+\sigma+q^2)^{1/2}\ , \tag{21}$$

satisfying

$$k^2+k-q^2-\sigma=0 \ . \tag{22}$$

We write the perturbed front position as

$$h^{(1)}=Ee^{iqx+\sigma t} \ . \tag{23}$$

When substituting Eqs. (20) and (23) into Eqs. (18e)–(18i), it is simpler to replace jump conditions (18h) and (18i) with the equivalent conditions

$$[(\partial^2-q^2)w^{(1)}]_-^+=0 \tag{24}$$

and

$$[(\partial^2+\partial-q^2-\sigma)\partial w^{(1)}]_-^+=-\delta_1 q^2 \mathcal{G} h^{(1)} \ . \tag{25}$$

This yields a linear algebraic system for the onset of convection,

$$LU=0 \ , \tag{26a}$$

where

$$L=\begin{bmatrix} -1 & -1 & 0 & 0 & \sigma+\mathcal{D}_C q^2 \\ 1 & 1 & -1 & -1 & 0 \\ q & -k_- & q & k_+ & 0 \\ 0 & \sigma-k_- & 0 & -\sigma+k_+ & 0 \\ \sigma+q & 0 & \sigma-q & 0 & -\delta_1 q \mathcal{G} \end{bmatrix} \tag{26b}$$

and

$$U=\begin{bmatrix} A \\ B \\ C \\ D \\ E \end{bmatrix} , \tag{26c}$$

and we have used Eq. (22) to simplify the fourth and fifth rows of $L$. Setting the determinant of $L$ to zero yields an eigenvalue condition

$$[q+2\sigma(q-s)]q\delta_1\mathcal{G}-4s(\sigma+\mathcal{D}_C q^2)(q^2-\sigma^2)=0 \ , \tag{27}$$

where $s=(\frac{1}{4}+\sigma+q^2)^{1/2}$. Equation (27) gives the growth rate $\sigma$ for a perturbation wave number $q$, an ascending front, and infinite thermal diffusivity.

### B. Zero thermal diffusivity

For $\mathcal{D}_T \to 0$, Eq. (15b) implies uniform unperturbed temperatures $\theta^{(0)}=\theta_0$ and $\theta^{(0)}=\theta_1$ in the unreacted and reacted fluids, respectively. Thus, in this limit, the temperature is discontinuous at the front, consistent with the inability of heat to diffuse into the unreacted fluid. Consequently, as for infinite thermal diffusivity, the density for zero thermal diffusivity is piecewise uniform, with values $\rho_0$ and $\tilde{\rho}_1$ in the unreacted and reacted fluids, respectively. Hence the stability problem is again governed solely by a discontinuous jump in density at the front, characterized here by the overall fractional density difference $\delta_0=\delta_1+\Delta\theta$ which includes the contribution $\Delta\theta$ from thermal expansion.

To account for all density differences for zero thermal diffusivity, it is simplest to include the piecewise uniform temperature in a redefined reduced pressure [see Eq. (12)],

$$P_r=P+\gamma[1-\alpha(T-T_1)]\rho_1 gz \ . \tag{28}$$

This reduced pressure leads to a factor $\delta_0$ instead of $\delta_1$ in Eq. (13g) and in all subsequent equations. Consequently, by replacing $\delta_1$ by $\delta_0$ in Eq. (27), we immediately obtain the eigenvalue condition for zero thermal diffusivity,

$$[q+2\sigma(q-s)]q\delta_0\mathcal{G}-4s(\sigma+\mathcal{D}_C q^2)(q^2-\sigma^2)=0 \ , \tag{29}$$

where $s=(\frac{1}{4}+\sigma+q^2)^{1/2}$ as before.

### C. Finite thermal diffusivity

The problem of finite thermal diffusivity is complicated because of temperature gradients near the front, which render the coefficient of $w^{(1)}$ in Eq. (18d) nonuniform and raise questions about how to account for all density differences. Although it may be useful to solve the finite-diffusivity problem, calculated growth rates for infinite and zero thermal diffusivity are expected to give approximate bounds on the growth rate for finite diffusivity when $\delta_1$ and $\Delta\theta$ are positive. Furthermore, as discussed below, these calculations are sufficient to make a successful first comparison with experiments.

## V. RESULTS AND DISCUSSION

By solving Eq. (27) numerically using parameter values in Table I, we obtain the dimensionless growth rate $\sigma$ as a function of the dimensionless wave number $q$ for infinite thermal diffusivity (Fig. 3, trace *a*). This growth rate of small perturbations about an ascending planar horizontal

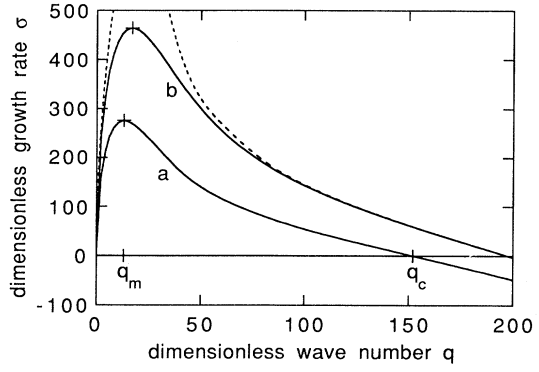


FIG. 3. Predicted variation of the dimensionless growth rate $\sigma$ with dimensionless wave number $q$ for infinite thermal diffusivity (trace *a*) and for zero thermal diffusivity (trace *b*) given by Eqs. (27) and (29) based on values of physical constants in Table I. The wave number $q_m$ of maximum growth rate and the wave number $q_c$ of zero growth rate from Eqs. (36) and (31) are shown for infinite thermal diffusivity. Asymptotic results for $q \to 0$ and $q \approx q_c$ given by Eqs. (41) and (39) are shown for zero thermal diffusivity (dashed traces). The symbols + locate the maxima predicted by Eqs. (36), (37), (42), and (43).

reaction front is relevant when the reacted fluid below the front is lighter than the unreacted fluid above the front ($\delta_1 > 0$). Indeed, upward propagation is unstable to long-wavelength perturbations with $q < q_c$, where $q_c = 152$ is a critical wave number for onset of convection. The curvature dependence of the normal front velocity [see Eq. (6)] stabilizes short-wavelength perturbations with $q > q_c$. The growth rate in Fig. 3 has the same basic features as the growth rate for perturbations about a planar horizontal Rayleigh-Taylor interface between two immiscible fluids,[5] where surface tension stabilizes the interface at short wavelengths.

The uniform-density approximation omits small density changes due to the different compositions of the reacted and unreacted fluids except where they modify gravity. A separate calculation[23] including all such changes yields no discernible change in Fig. 3.

We have also calculated the growth rate for zero thermal diffusivity, obtained from Eq. (29) using parameter values from Table I (Fig. 3, trace *b*). Clearly, the larger fractional density difference $\delta_0 = 1.9 \times 10^{-4}$ for zero thermal diffusivity (compared with $\delta_1 = 0.87 \times 10^{-4}$ for infinite thermal diffusivity) implies a larger band of unstable wavelengths, with a critical wave number $q_c = 197$ for onset of convection. Critical wave numbers for finite thermal diffusivity might lie between this value and the value $q_c = 152$ for infinite thermal diffusivity.

In the absence of an explicit general solution for $\sigma$ from Eq. (27), it is instructive to obtain asymptotic solutions in regions of physical interest. For $q^2$ large compared with $\frac{1}{4}$, $\sigma$, and $\sigma^2$ near the onset of convection, Eq. (27) with $s = q$ yields the near-critical growth rate

$$\sigma = \frac{\delta_1 \mathcal{G}}{4q} - \mathcal{D}_C q^2 \quad (q \approx q_c) \tag{30}$$

and the corresponding critical wave number

$$q_c = \left[ \frac{\delta_1 \mathcal{G}}{4\mathcal{D}_C} \right]^{1/3} . \tag{31}$$

Substituting values from Table I into Eq. (31), we easily recover the computed value $q_c = 152$, with corrections to Eq. (31) of relative order $1/4q_c^2 \approx 10^{-5}$. Small $\sigma$ near $q_c$ implies that time scales for relaxation of disturbances near the critical wave number are very long. This phenomenon of "critical slowing down" near the onset of convection is familiar in phase transitions and in Rayleigh-Bénard convection.

For an infinite fractional density difference $\delta_1 \to \infty$ and upward propagation, Eq. (31) implies that all wavelengths become unstable to convection. This result reflects the dominance of buoyant forces over the stabilizing effects of curvature for large density differences. Since $q_c$ decreases with decreasing $\delta_1$, the approximation $q^2 \gg \frac{1}{4}$ in Eqs. (30) and (31) eventually breaks down for small enough $\delta_1$. As $q^2$ decreases through the value $\frac{1}{4}$, Eq. (31) crosses over to $q_c = (\delta_1 \mathcal{G}/2\mathcal{D}_C)^{1/2}$ valid for $\delta_1 \to 0$, obtained by setting $\sigma = 0$ in Eq. (27) with $q^2 \ll \frac{1}{4}$. Thus $q_c \to 0$ as $\delta_1 \to 0$, implying that the flat front is stable to perturbations of all wavelengths in the limit of zero density difference between the fluids, as expected. Clearly, the flat front (with $\mathcal{D}_T \to \infty$) must also be stable when $\delta_1 < 0$, that is, when the reacted fluid below the front is heavier than the unreacted fluid.

For finite $\delta_1$, Fig. 3 implies that the growth rate $\sigma$ vanishes in the limit of long wavelengths, that is, as $q \to 0$. Accordingly, using Eq. (27) with $\sigma$ small compared with $\frac{1}{4}$ but large compared with $q$, $\mathcal{D}_C q^2$, and $q^2$, we find that $\sigma$ vanishes as the square root of the wave number as $q \to 0$;

$$\sigma = \left[ \frac{\delta_1 \mathcal{G} q}{2} \right]^{1/2} \quad (q \to 0) . \tag{32}$$

The maximum growth rate $\sigma_m$ and the corresponding wave number $q_m$ are interesting because a planar horizontal front subjected to random thermal or mechanical perturbations is expected to select a perturbation wave number $q$ near $q_m$ and a corresponding growth rate $\sigma$ near $\sigma_m$. The values $q_m = 13.01$ and $\sigma_m = 275.69$ obtained numerically from Eq. (27) satisfy $\sigma \gg \frac{1}{4}$, $\sigma \gg \mathcal{D}_C q^2$, and $\sigma^2 \gg q^2$. With these approximations, Eq. (27) reduces to

$$2s\sigma^2 = (s - q) q \delta_1 \mathcal{G} , \tag{33}$$

with $s = (\sigma + q^2)^{1/2}$, valid for $q \approx q_m$. We can take the first derivative of Eq. (33) with respect to $q$ and set $d\sigma/dq = 0$ to find a relation between $\sigma_m$ and $q_m$,

$$\frac{2q_m}{\delta_1 \mathcal{G}} \sigma_m^2 = (s_m - q_m)^2 , \tag{34}$$

where $s_m = (\sigma_m + q_m^2)^{1/2}$. A useful relation for $\sigma_m$,

$$\sigma_m = \frac{\delta_1 \mathcal{G}}{2q_m} - (2\delta_1 \mathcal{G} q_m)^{1/2}, \tag{35}$$

follows by taking the square root of Eq. (34), solving for $s_m$, squaring, and simplifying. It is convenient to set

$$q_m = a(\delta_1 \mathcal{G})^{1/3} , \tag{36}$$

where $a$ is a constant, so that Eq. (35) yields

$$\sigma_m = b(\delta_1 \mathcal{G})^{2/3} , \tag{37}$$

with $b = 1/2a - (2a)^{1/2}$ a function of $a$ only. Substituting these relations into Eq. (33) yields an expression independent of $\delta_1$ and $\mathcal{G}$,

$$4a^{9/2} - 7(2)^{1/2} a^3 + 5a^{3/2} - 2^{-1/2} = 0 , \tag{38}$$

hence $a$ and $b$ are pure numbers independent of any physical parameters. Solving Eq. (38) numerically produces the universal values $a = 0.417\,836\,60$ and $b = 0.282\,488\,40$. Consequently, inserting values from Table I into Eqs. (37) and (36) yields the maximum growth rate $\sigma_m = 275.98$ and the corresponding wave number $q_m = 13.06$ ("+" symbol at the peak of trace *a*, Fig. 3), in excellent agreement with the values $\sigma_m = 275.69$ and $q_m = 13.01$ obtained numerically from Eq. (27).

Owing to the similarity between Eqs. (27) and (29), we

can immediately deduce the asymptotic solutions and critical values for zero thermal diffusivity from their counterparts for infinite thermal diffusivity, Eqs. (30)–(32), (36), and (37). Thus

$$\sigma=\frac{\delta_0\mathcal{G}}{4q}-\mathcal{D}_C q^2 \quad (q\approx q_c)\,, \tag{39}$$

$$q_c=\left[\frac{\delta_0\mathcal{G}}{4\mathcal{D}_C}\right]^{1/3}, \tag{40}$$

$$\sigma=\left[\frac{\delta_0\mathcal{G}q}{2}\right]^{1/2} \quad (q\to 0)\,, \tag{41}$$

$$q_m=a(\delta_0\mathcal{G})^{1/3}\,, \tag{42}$$

$$\sigma_m=b(\delta_0\mathcal{G})^{2/3}\,, \tag{43}$$

where $a=0.417\,836\,60$ and $b=0.282\,488\,40$ as before. In all cases, approximations used in the preceding paragraphs to arrive at the results for infinite thermal diffusivity are equally well or better justified here. In Fig. 3, dashed traces show the asymptotic forms (39) and (41), and a "+" symbol locates the maximum given by Eqs. (42) and (43).

It is instructive to compute the velocity field of the instability leading to convection for zero thermal diffusivity. (Infinite thermal diffusivity yields a similar field.) At onset of convection, this can be accomplished by replacing $\delta_1$ by $\delta_0$, by setting $\sigma=0$, $q=q_c=197.3242$, and $E=1$, and by eliminating the fifth row in the linear system, Eq. (26a). The resulting fourth-order inhomogeneous system yields the remaining coefficients $A=3.3345\times10^4$, $B=-3.3261\times10^4$, $C=-3.3345\times10^4$, and $D=3.3430\times10^4$, so that the imaginary parts of Eqs. (18a), (20), and (23) give explicit relations for the horizontal and vertical components of velocity and for the front shape. Figure 4 shows one horizontal period of the resulting velocity field for perturbations of wavelength $\lambda=\lambda_c=2\pi/q_c=3.18\times10^{-2}$ about a planar horizontal front; the sinusoidal trace represents the position of the perturbed front.

As is evident in Fig. 4, the fluid velocity vanishes exponentially with vertical distance from the front, and fluid motion is restricted principally to the region defined by $-\lambda/2<z<\lambda/2$. The flow forms cells analogous to Rayleigh-Bénard cells, where upflow (downflow) tends to carry the front upward (downward). At onset of convection where $\sigma=0$, this tendency is exactly balanced by the reduction (enhancement) of the front velocity for upward (downward) displacements, thus producing a steady curved front. Without the curvature dependence in the front velocity [see Eq. (6)] responsible for these reductions and enhancements, this balance could not be achieved for infinitesimal perturbations, and all wavelengths would become unstable. This can also be seen by taking $\mathcal{D}_C=0$ in Eq. (31). The higher curvature associated with short-wavelength perturbations with $\lambda<\lambda_c$ and finite $\mathcal{D}_C$ overwhelms the tendency for the fluid to displace the front, so that the front remains flat. These short-wavelength perturbations decay with time because a flat front provides no reduction in the overall gravitational potential energy. Thus the curvature dependence of the front velocity in Eq. (6) is crucial to the understanding of the onset of convection in autocatalytic systems.

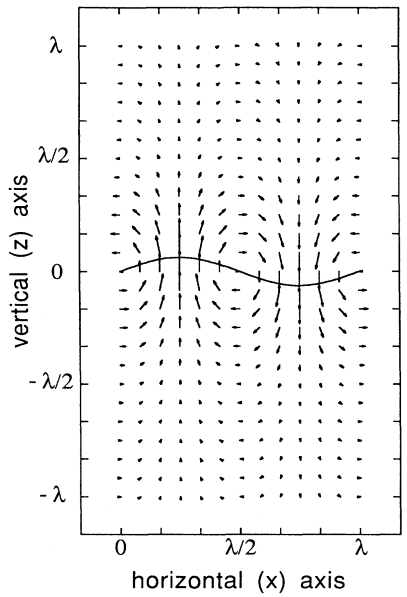


FIG. 4. Velocity field at the onset of convection for perturbations of critical wavelength $\lambda=\lambda_c$ about a flat ascending horizontal autocatalytic reaction front in a laterally unbounded system for zero thermal diffusivity. The sinusoidal trace represents the position of the perturbed front.

## VI. COMPARISON WITH EXPERIMENTS

To allow for comparison with experiments, it is helpful to write the principal results of the paper in conventional units. Recalling the length, time, and temperature scales $\nu/c_0$, $\nu/c_0^2$, and $\alpha^{-1}$, using the definitions in Table I, and defining a wave number $\tilde{q}=c_0\nu^{-1}q$, growth rate $\tilde{\sigma}=c_0^2\nu^{-1}\sigma$, and wavelength $\tilde{\lambda}=2\pi/\tilde{q}$ in conventional units, we can rewrite the steady temperature profile for the undisturbed ascending front and arbitrary thermal diffusivity, Eq. (15b), as

$$T^{(0)}=\begin{cases}T_0+(T_1-T_0)e^{-(z-z_0)/d_T}, & z>z_0\\ T_1, & z<z_0\,,\end{cases} \tag{44}$$

where $z$ is once again measured in conventional units and $z=z_0$ is the location of the undisturbed front in the moving frame. We can also rewrite Eqs. (39)–(43) for zero thermal diffusivity as

$$\tilde{\sigma}=\frac{\delta_0 g}{4\nu\tilde{q}}-D_C\tilde{q}^{\,2} \quad (\tilde{q}\approx\tilde{q}_c)\,, \tag{45}$$

$$\tilde{q}_c=\left[\frac{\delta_0 g}{4\nu D_C}\right]^{1/3}, \tag{46}$$

$$\tilde{\sigma}=\left[\frac{\delta_0 g\tilde{q}}{2}\right]^{1/2} \quad (\tilde{q}\to 0)\ , \tag{47}$$

$$\tilde{q}_m=a\left[\frac{\delta_0 g}{\nu^2}\right]^{1/3}\ , \tag{48}$$

$$\tilde{\sigma}_m=b\left[\frac{\delta_0 g}{\nu^{1/2}}\right]^{2/3}\ , \tag{49}$$

where $a=0.417\,836\,60$ and $b=0.282\,488\,40$ as before. Results for infinite thermal diffusivity follow by replacing $\delta_0$ by $\delta_1$ in these equations.

None of the limiting forms (45)–(49) depends on the planar front speed $c_0$, indicating that the slow front speed is unimportant at the onset of convection. Written in conventional units, the linearized equations depend on $c_0$ only through the convective term $[\mathbf{V}^{(0)}\cdot\nabla]\mathbf{V}^{(1)}=-c_0\partial\mathbf{V}^{(1)}/\partial z$. The small magnitude $c_0 d/\nu\approx 3\times 10^{-2}$ of this term relative to the viscous term $\nu\nabla^2\mathbf{V}^{(1)}$ [see Eq. (13a)] indicates the insignificance of the convective term, although the actual corrections due to this term are much smaller (of order $10^{-3}$–$10^{-5}$; see Sec. V). Neglecting the convective term and accordingly replacing Eq. (25) with Eq. (18i) leads to a simpler eigenvalue condition for zero thermal diffusivity [compare Eq. (29)],

$$\frac{q}{(\sigma+q^2)^{1/2}}+\frac{2(\sigma+\mathcal{D}_C q^2)\sigma}{\delta_0 q\,\mathcal{G}}-1=0\ . \tag{50}$$

Carrying out the arguments in Sec. V with this $c_0$-independent condition again yields the limiting forms (45)–(49).

Figure 5 shows the undisturbed temperature profile given by Eq. (44) (solid trace) compared with experimental measurements (data points) from Fig. 3.5a of Ref. 1 for upward propagation and reaction mixture "*D*." The thermal length scale $d_T=D_T/c_0=1.83$ mm giving the spatial decay of the temperature in Eq. (44) follows from the thermal diffusivity $D_T=1.45\times 10^{-3}$ cm$^2$/s from Table I and the value $c_0=0.007\,91$ cm/s inferred from Figs. 3.2a and 3.5a of Ref. 1. Fitting Eq. (44) to the experimental points yields the values $T_0=22.16$ °C, $T_1=23.06$ °C, and $z_0=3.4$ mm. Clearly, the predicted temperature profile for a thin undisturbed front (with discontinuous slope at the front) agrees with the experimental profile for upward propagation except for a small amount of rounding near the front due to the finite thickness of the front. Perturbations in the temperature profile associated with the convective flow near onset (which have not been calculated since only $D_T=0$ and $\infty$ have been considered) are expected to yield small perturbations about the predicted undisturbed profile near onset of convection. The exponential decay of the temperature ahead of the front is responsible for density gradients in the vicinity of the front shown schematically in Fig. 1.

When the uniform density of the unreacted fluid is greater than that of the unreacted fluid in a laterally unbounded system, linear stability theory predicts that convection can occur only for upward propagation with wavelengths exceeding a critical wavelength $\tilde{\lambda}_c=2\pi/\tilde{q}_c$, with $\tilde{q}_c$ given by Eq. (46). For experimental parameters in Table I relevant to iodate–arsenous acid solutions, we predict $\tilde{\lambda}_c=0.99$ mm for dimensionless thermal diffusivity $\mathcal{D}_T=D_T/\nu=0$ and $\tilde{\lambda}_c=1.29$ mm for $\mathcal{D}_T\to\infty$. (These values correspond respectively to the dimensionless wave numbers $q_c=197$ and 152 discussed in Sec. V.) We expect the critical wavelength for finite $\mathcal{D}_T$ to lie near these values.

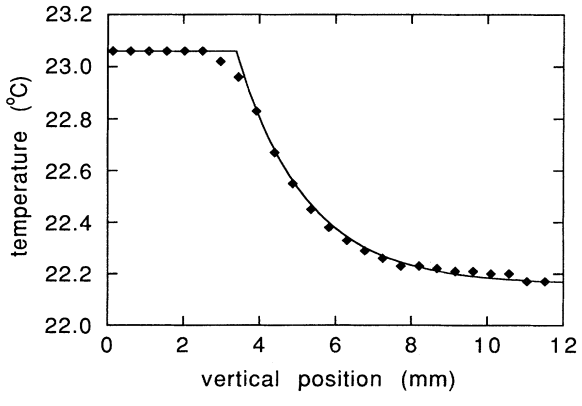


FIG. 5. Experimental (data points) and theoretical (solid trace) variation of temperature with height in the absence of convection in a frame stationary with respect to the ascending front. Experimental data are from Ref. 1, Fig. 3.5a. The theoretical variation is given by Eq. (44).

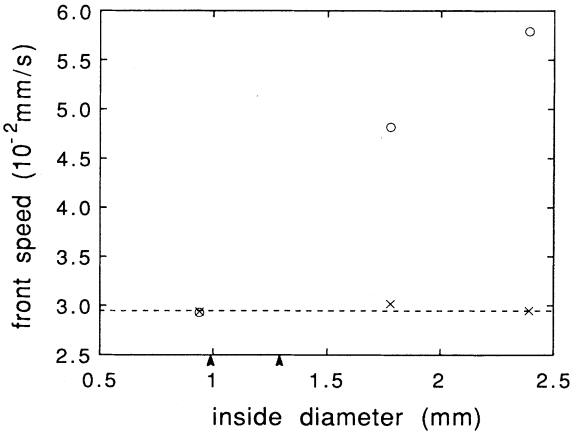


FIG. 6. Experimental front propagation speeds for upward propagation (○) and downward propagation (×) as a function of tube diameter for an iodate–arsenous acid solution (reaction mixture "*A*," Table 3.4 of Ref. 1 corresponding to Table 4 of Ref. 3). The dashed line gives the estimated downward propagation speed $c_0=2.95\times 10^{-2}$ mm/s. The ascending speed first deviates significantly from the descending speed at a critical diameter for the onset of convection between the diameters 0.94 and 1.78 mm. The arrow heads give the predicted critical wave numbers $\tilde{\lambda}_c=0.99$ and 1.29 mm for the onset of convection in a laterally unbounded system for zero and infinite dimensionless thermal diffusivity $\mathcal{D}_T=D_T/\nu$, respectively.

This predicted critical wavelength can be compared with the experiments on iodate–arsenous acid systems.[1,3] Measurements of the descending front propagation speed versus tube diameter ("×" symbols in Fig. 6) imply a convectionless flat front speed $c_0=(2.95\pm0.04)\times10^{-2}$ mm/s (dashed line). Since front propagation speeds in excess of $c_0$ imply convection [Eq. (5)], measurements of the ascending front propagation speed ("○" symbols) exclude convection for $d\leq0.94$ mm and imply convection for $d\geq1.78$ mm. Accordingly, the experiments imply convection in vertical tubes only for upward propagation with diameters exceeding a critical diameter $d_c$ in the range $0.94\text{ mm}<d_c<1.78$ mm. This measured range includes the predicted range $0.99\text{ mm}<\tilde{\lambda}_c<1.29$ mm, whose end points are denoted by arrow heads in Fig. 6. Hence the predicted horizontal length scale $\tilde{\lambda}_c$ for the onset of convection in a laterally unbounded system agrees with the observed horizontal length scale $d_c$ for the onset of convection in vertical tubes.

## VII. CONCLUSIONS

A linear analysis of infinitesimal-amplitude convection near autocatalytic reaction fronts in a laterally unbounded geometry predicts an undisturbed temperature profile which agrees with experiments and a critical minimum wavelength for onset of stationary convection. This critical wavelength agrees with the observed critical diameter for upward propagation in long vertical cylinders filled with iodate–arsenous acid solutions.[1] This agreement motivates calculations for cylindrical geometries, which are currently under way.

Precise measurements of the critical diameter for the onset of convection would be very helpful in connection with ongoing calculations for cylindrical geometries. For reaction mixture "$A$" relevant to Fig. 6, this could be accomplished by measuring the front speed for several tube diameters in the range $0.94\text{ mm}<d<1.78$ mm. It should also be helpful to measure the critical diameter for other reaction mixtures. Since a transition to increased front speed heralds the onset of convection, the onset of convection could also be located by a series of measurements of the front speed for constant tube diameter and varying reactant concentrations.

Measurements of the maximum growth rate $\tilde{\sigma}_m$ and the corresponding wavelength $\tilde{\lambda}_m=2\pi/\tilde{q}_m$ would also be helpful. The experiments could be carried out by initiating a reaction at the bottom of a cylinder (or other container) and by comparing the width and growth rate of developing features in the front with $\tilde{\lambda}_m$ and $\tilde{\sigma}_m$. For the data in Table I, Eqs. (48) and (49) predict the ranges $1.2\text{ cm}<\tilde{\lambda}_m<1.5$ cm and $0.26\text{ s}^{-1}<\tilde{\sigma}_m<0.44\text{ s}^{-1}$ based on values at zero and infinite thermal diffusivity. The cylinder diameter for the experiments should be large compared with $\tilde{\lambda}_m$ to allow the front to choose its own length scale independent of the sidewalls.

When the reacted fluid is lighter than the unreacted fluid, the linear stability of a flat ascending autocatalytic reaction front is similar to a flat Rayleigh-Taylor interface between two immiscible fluids of differing densities: both interfaces are unstable above a critical wavelength for the onset of convection. The essential differences between these problems lie in the nature of the interface between the fluids. For autocatalytic reaction fronts, the conversion of unreacted fluid into reacted fluid by the interface necessarily involves a nonzero interface velocity with respect to the fluids, whereas impermeable Rayleigh-Taylor interfaces are stationary with respect to the fluids. As a result, surface tension $\tau$ renders the stress discontinuous and tends to stabilize the interface only in the Rayleigh-Taylor problem, leading to a critical wave number for the onset of convection $[(\rho_u-\rho_l)g/\tau]^{1/2}$ that involves the density difference between the upper and lower fluids. The viscous and nonviscous Rayleigh-Taylor problems both yield this same critical wave number,[5] which is manifestly independent of the fluid viscosity $\nu$. In autocatalytic reactions, it is the curvature dependence of the interface velocity that tends to stabilize the interface, leading to a viscosity-dependent critical wave number $[(\rho_u-\rho_l)g/4\rho_l\nu D_C]^{1/3}$ that involves the catalyst diffusivity $D_C$ and the buoyancy parameters $(\rho_u-\rho_l)g$ raised to the power 1/3 rather than 1/2. These differences clearly distinguish the problem of a propagating autocatalytic reaction front from the classical viscous Rayleigh-Taylor problem.

The small calculated variation in the critical wavelength as the thermal diffusivity goes from zero to infinity implies that the system behavior is dominated by the discontinuous jump in density at the front rather than by thermal gradients (for upward propagation and a reacted fluid that is lighter than the unreacted fluid). However, when the reacted fluid is heavier than the unreacted fluid, this jump in density stabilizes the front for upward propagation. Thus it may be possible in this case to observe a transition to convection driven by thermal gradients analogous to the Rayleigh-Bénard instability of a fluid heated from below. This problem is currently under investigation.

## ACKNOWLEDGMENTS

Insightful discussions with Alan Kerstein, James Maher, and Stephen Margolis are gratefully acknowledged. We are grateful to Terence McManus for providing tabulated data for Fig. 5. This work was supported in part by National Science Foundation Grant Nos. RII-8922106, CHE-8311360, and CHE-8920664 and the West Virginia University Energy and Water Research Center.

[1]T. McManus, Ph. D. thesis, West Virginia University, Chap. 3, 1989.

[2]J. A. Pojman and I. R. Epstein, J. Phys. Chem. **94**, 4966 (1990).

[3]J. A. Pojman, I. R. Epstein, T. J. McManus, and K. Showalter, J. Phys. Chem. (to be published).

[4]A. Saul and K. Showalter, in *Oscillations and Traveling Waves in Chemical Systems,* edited by R. J. Field and M. Burger (Wiley, New York, 1985), p. 419; N. Ganapathisubramanian

and K. Showalter, J. Chem. Phys. **84**, 5427 (1986).
[5]S. Chandrasekhar, *Hydrodynamic and Hydromagnetic Stability* (Oxford University Press, London, 1961), Chap. 10.
[6]H. Bénard, Rev. Gen. Sci. Pure Appl. **11**, 1261 (1900); **11**, 1309 (1900); H. Bénard, Ann. Chim. Phys. **23**, 62 (1901); Lord Rayleigh, Philos. Mag. **32**, 529 (1916).
[7]G. Ahlers, in *Complex Systems, Vol. 7, Sante Fe Institute Studies in the Sciences of Complexity,* edited by D. Stein (Addison, Reading, MA 1989).
[8]A. Schlüter, D. Lortz, and F. Busse, J. Fluid Mech. **23**, 129 (1965); M. C. Cross, Phys. Fluids **23**, 1727 (1980); B. F. Edwards and A. L. Fetter, *ibid.* **27**, 2795 (1984).
[9]S. Chandrasekhar, *Hydrodynamic and Hydromagnetic Stability* (Ref. 5), Chap. 2.
[10]B. F. Edwards, J. Fluid Mech. **191**, 583 (1988).
[11]L. Landau, Acta Physicochim. URSS **19**, 77 (1944).
[12]Z. Rakib and G. I. Sivashinsky, Combust. Sci. Technol. **54**, 69 (1987).
[13]M. Matalon and B. J. Matkowsky, Combust. J. Fluid Mech. **124**, 239 (1982); M. Matalon and B. J. Matkowsky, Combust. Sci. Technol. **34**, 295 (1983).
[14]G. H. Markstein, *Nonsteady Flame Propagation* (Pergamon, Oxford, 1964).
[15]P. pelce and P. Clavin, J. Fluid Mech. **124**, 219 (1982).
[16]A. Hanna, A. Saul, and K. Showalter, J. Am. Chem. Soc. **104**, 3838 (1982).
[17]G. I. Taylor, Proc. R. Phys. Soc. London Ser. B **67**, 857 (1954).
[18]E. L. Cussler, *Diffusion: Mass transfer in fluid systems,* (Cambridge University Press, New York, 1984), Chap. 12.
[19]J. Boussinesq, *Théorique Analytique de la Chaleur* (Gauthier-Villars, Paris, 1903), Vol. 2; A. Oberbeck, Ann. Phys. Chem. (Leipzig) **7**, 271 (1879); A. Oberbeck, Sitzungsberg, Berl. Kl. Preuss. Akad. Wiss. 383 (1888); 1129 (1888).
[20]J. S. Langer, Rev. Mod. Phys. **52**, 1 (1980).
[21]J. A. Pojman, I. P. Nagy, and I. R. Epstein (unpublished).
[22]G. Bazsa and I. R. Epstein, J. Phys. Chem. **89**, 3050 (1985).
[23]B. F. Edwards, J. W. Wilder, and K. Showalter (unpublished).
[24]I. Nagypál, G. Bazsa, and I. R. Epstein, J. Am. Chem. Soc. **108**, 3635 (1986).
[25]G. I. Taylor, Philos. Trans. R. Soc. London Ser. A **223**, 289 (1923); R. C. DiPrima and H. L. Swinney, in *Hydrodynamic Instabilities and the Transition to Turbulence,* edited by H. L. Swinney and J. P. Gollub (Springer, Berlin, 1981).
[26]J. J. Tyson and J. P. Keener, Physica D **32**, 327 (1988).
[27]A. L. Fetter and J. D. Walecka, *Theoretical Mechanics of Particles and Continua* (McGraw-Hill, New York, 1980), Chaps. 9 and 12.
[28]*CRC Handbook of Chemistry and Physics,* edited by R. C. Weast and M. J. Astle (CRC, Boca Raton, FL, 1978), Sec. F-5.